Geochemistry Geophysics Geosystems G3

Article
Volume 13, Number 1
6 January 2012
Q01002, doi:10.1029/2011GC003859
ISSN: 1525-2027

Published by AGU and the Geochemical Society

The role of the overriding plate thermal state on slab dip variability and on the occurrence of flat subduction

Juan Rodríguez-González and Ana M. Negredo
Departamento de Geofísica y Meteorología, Universidad Complutense de Madrid, E-28004 Madrid, Spain (juan.rodriguez@fis.ucm.es; anegredo@fis.ucm.es)

Instituto de Geociencias, UCM-CSIC, E-28040 Madrid, Spain

Magali I. Billen
Department of Geology, University of California, Davis, California 95616, USA

[1] Slab dip varies significantly, both between different, and along single subduction zones. Provided that old subducting plates are colder and denser than young plates, variations in the slab dip should correlate with slab age. However, recent statistical analyses do not show this expected correlation. We present the results of non-Newtonian numerical dynamic models where subduction is driven by means of a kinematic boundary condition. We systematically vary the age of both the overriding and subducting plates in order to test these effects on the slab dip at different depth ranges. We find that colder overriding plates result in shallower slab dips and episodes of flat slab subduction, as a result of the increased suction force in the mantle wedge. The influence of the thermal state of the overriding plate on slab dip is shown here to be more important than that of the age of subducting lithosphere. Modeling results are qualitatively compared to the large dip variability of the Cocos slab including a flat-slab segment. We suggest that this variability is likely related to the change of the thermal state of the overriding plates, with flat subduction occurring under cold lithosphere in southwestern Mexico and steep subduction under the warmer lithosphere of the northwestern Caribbean plate.

Components: 13,200 words, 9 figures, 2 tables.

Keywords: Cocos plate; flat subduction; slab buoyancy; slab dip; subduction dynamics; thermomechanical numerical modeling.

Index Terms: 8120 Tectonophysics: Dynamics of lithosphere and mantle: general (1213); 8170 Tectonophysics: Subduction zone processes (1031, 3060, 3613, 8413).

Received 7 September 2011; **Revised** 15 November 2011; **Accepted** 15 November 2011; **Published** 6 January 2012.

Rodríguez-González, J., A. M. Negredo, and M. I. Billen (2012), The role of the overriding plate thermal state on slab dip variability and on the occurrence of flat subduction, *Geochem. Geophys. Geosyst.*, *13*, Q01002, doi:10.1029/2011GC003859.

1. Introduction

[2] Subducting lithosphere (slabs) constitutes one of the main driving forces for plate motions, yet how slabs deform and transmit stresses to the subducting plate remains unclear [*Conrad and Hager*, 1999; *Conrad and Lithgow-Bertelloni*, 2002; *Buffett and Rowley*, 2006; *Billen and Hirth*, 2007; *Ribe*, 2010]. The ability of slabs to transmit buoyancy forces to the subducting plate depends on the rheology of the slab and mantle, as well as evolution of slab dip (i.e., component of slab buoyancy force

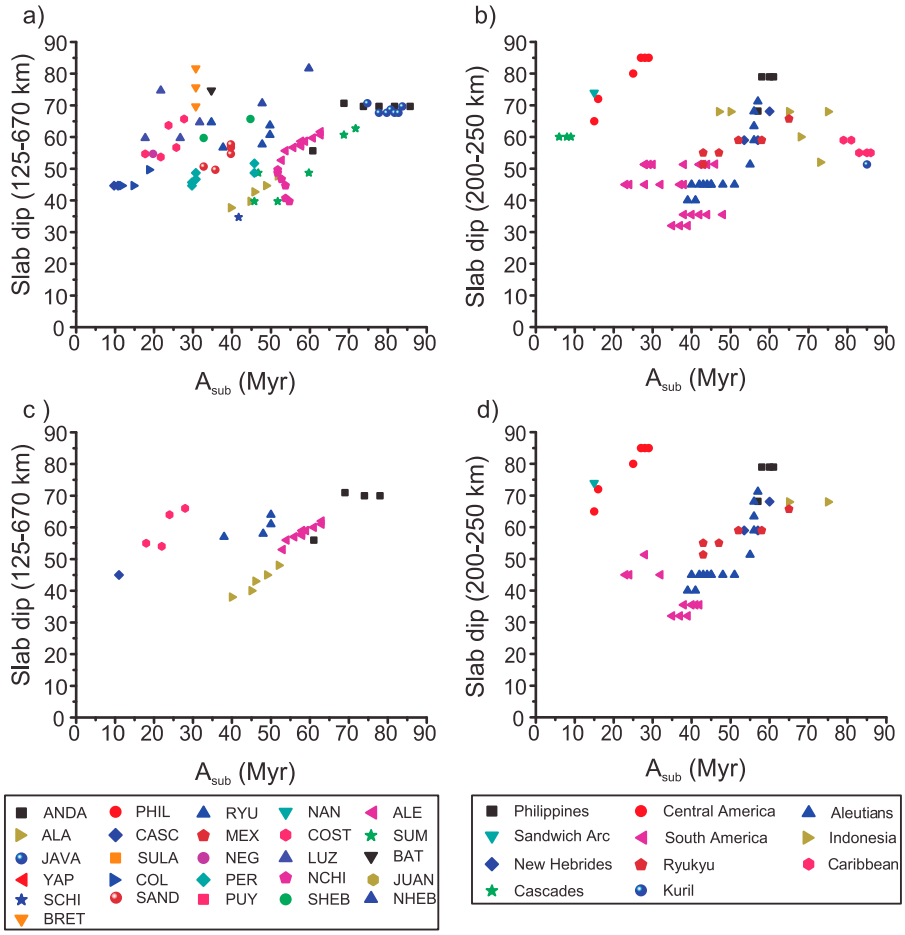

Figure 1. Slab dip as function of the age of the subducting plate at the trench, with data measured along transects perpendicular to the trench. Original data from (a) *Lallemand et al.* [2005] (89 transects) and (b) *Cruciani et al.* [2005] (94 transects) show only a weak correlation. (c, d) These figures show a strong correlation for the same data as in Figures 1a and 1b after removing 56 and 45 points, respectively, representing data from near-edge transects and from slabs that sink into the lower mantle.

[*Lallemand et al.*, 2005]) with time. Significant slab dip variability can be found between different subduction zones, or even along the same subduction zone (Figure 1) [*Isacks and Barazangi*, 1977; *Jarrard*, 1986; *Cruciani et al.*, 2005; *Lallemand et al.*, 2005]. Together with this variation in slab dip, four different styles of subduction have been described: flat subduction, in which the slab reverses its curvature and subducts almost horizontally for hundreds of kilometers, (e.g., Peru); low-angle subduction with slab dips lower than 30° (e.g., Cascades); intermediate-angle subduction, with slab dip between 30° and 60° (e.g., Ryukyu); and high-angle subduction with slab dip greater than 60° (e.g., Marianas). Around 10% of slabs subduct with very low angle, as for example the Nazca plate dipping about 15° under southern Peru [*Barazangi and Isacks*, 1979; *Jarrard*, 1986]. Flat subduction can also be found in central Chile [e.g., *Gutscher et al.*, 2000] and Central Mexico [e.g., *Suárez et al.*, 1990; *Pérez-Campos et al.*, 2008], where the flat segment is connected to a much steeper portion of the slab at depth. In some regions flat slab subduction is known to be caused by subduction of thick, buoyant crust (e.g., the Yakutat Block beneath southern Alaska [*Christeson et al.*, 2010]), while in other regions, such as Central Mexico, the causes are still debated. In addition, different geological observations indicate that the Farallon plate subducted underneath North America plate with a flat (or very low) angle about 65 Ma ago and may be responsible for tectonism far from the plate boundary [*Bird*, 1988; *Schmid et al.*, 2002; *Sigloch et al.*, 2008].

[3] The causes of slab dip variability remain unclear although several explanations have been proposed

and investigated with analytical [*Stevenson and Turner*, 1977; *Tovish et al.*, 1978; *Royden and Husson*, 2006; *Ribe*, 2010], numerical [e.g., *Billen*, 2008; *Di Giuseppe et al.*, 2008; *Tetzlaff and Schmeling*, 2009; *Capitanio et al.*, 2010, and references therein] and laboratory models [e.g., *Kincaid and Olson*, 1987; *Griffiths et al.*, 1995; *Guillou-Frottier et al.*, 1995; *Funiciello et al.*, 2003, 2006, 2008; *Schellart*, 2004; *Heuret et al.*, 2007; *Boutelier and Cruden*, 2008]. First, it has been proposed that slab dip is affected by the balance between the torque related to slab buoyancy and the torque exerted by hydrodynamic pressure caused by the flow generated under the slab and in the mantle wedge located between the slab and the base of the upper plate [*Stevenson and Turner*, 1977; *Tovish et al.*, 1978].

[4] Second, a number of studies show that slab geometry is significantly influenced by trench migration. In this sense, trench motion with respect to the upper plate is shown to be correlated with slab dip [*Uyeda and Kanamori*, 1979; *Jarrard*, 1986; *Lallemand et al.*, 2005], with advancing trenches generally corresponding to steeper slabs. Trench motion has been investigated either with models including a subducting and overriding plate [e.g., *Kincaid and Olson*, 1987; *Griffiths et al.*, 1995; *Zhong and Gurnis*, 1995; *Yamato et al.*, 2009; *van Dinther et al.*, 2010; *Quinquis et al.*, 2011] or considering only a subducting plate [e.g., *Christensen*, 1996; *Enns et al.*, 2005; *Stegman et al.*, 2006, 2010; *Schellart et al.*, 2007; *Faccenna et al.*, 2007].

[5] Third, the interaction between the subducting slab and a hypothetical large scale mantle flow has been proposed as responsible for the difference between eastward and westward dipping slabs [e.g., *Ricard et al.*, 1991; *Doglioni et al.*, 1999]. Although this slab-mantle flow interaction should significantly affect slab dip [*Olbertz and Wortel*, 1997; *Boutelier and Cruden*, 2008], no agreement about the relationship between slab polarity and dip has been reached in statistical analyses (e.g., *Cruciani et al.* [2005] and *Riguzzi et al.* [2009] versus *Lallemand et al.* [2005] and *Schellart* [2007]).

[6] Fourth, slab dip can be affected by the rheology of the slabs and the surrounding mantle [*Čížková et al.*, 2002; *Billen and Hirth*, 2005, 2007; *Bellahsen et al.*, 2005; *Manea and Gurnis*, 2007]. For example, lower viscosity slabs tend to evolve to steep dips, while high viscosity slabs tend to shallow once they enter a higher viscosity lower mantle. Finally, the effects of phase transition on the buoyancy of slabs can also affect evolution of slab dip with time [*Schmeling et al.*, 1999; *Tetzlaff and Schmeling*, 2000, 2009; *van Hunen et al.*, 2001].

[7] Despite all the possible processes that can perturb or even dominate slab dip, to first order slab dynamics can be understood as resulting from a balance of driving forces (slab buoyancy) and resisting forces (rheologically induced). For the evolving dip of the slab, this balance of forces can be discussed in terms of the expected influence of hydrodynamic (viscous) and buoyancy forces on slab dip, while keeping the trench fixed. The gravitational torque per unit slab width t_G resulting from the slab buoyancy of a rigid slab sinking at an angle α is

$$t_G = \frac{T_G}{D} = \int_0^l \Delta\rho(r,\alpha) g h r \cos\alpha \, dr \tag{1}$$

where D is the slab width, $\Delta\rho$ is the density contrast between the slab and the mantle, l is the length of the slab, h is the thickness of the plate and r is the radial coordinate with the origin placed at the base of the lithosphere in the plate boundary. This torque is mainly controlled by the buoyancy of the slab, and thus, it is expected that older (so colder and denser) lithosphere, will subduct more steeply than younger lithosphere. The gravitational torque is balanced by the hydrodynamic torque per unit slab width t_H, which exerts a suction force on the slab,

$$t_H = \frac{T_H}{D} = \int_0^l [P_A(\theta,r) - P_B(\theta,r)] r dr \tag{2}$$

where P_A and P_B are the pressures beneath and above the slab, respectively. *McKenzie* [1969] obtained the following expression for P_A and P_B assuming constant mantle viscosity and a linear geometry of the slab:

$$\mathrm{P_A}(\alpha) = \frac{2\eta_\mathrm{W} \mathrm{u_s} \sin(\alpha)}{\mathrm{r}(\pi - \alpha) + \sin(\alpha)} \tag{3}$$

$$\mathrm{P_B}(\alpha) = -\frac{2\eta_\mathrm{W} \mathrm{u_s} \sin^2\alpha}{\mathrm{r}(\alpha^2 - \sin^2\alpha)} \tag{4}$$

where η_W is the viscosity in the mantle wedge, α is the slab dip and u_s the subduction velocity. This leads to the following analytical solution for the suction torque [*Stevenson and Turner*, 1977]:

$$t_H = 2\eta_W u_s l \left[\frac{\sin\alpha}{(\pi - \alpha) + \sin\alpha} + \frac{\sin^2\alpha}{\alpha^2 - \sin^2\alpha} \right] \tag{5}$$

As can be seen in equation (5), this torque strongly depends on the viscosity of the mantle wedge and the slab dip [*Stevenson and Turner*, 1977; *Tovish et al.*, 1978]. For higher viscosity or smaller dip angles, the hydrodynamic torque causes increased upward suction of the slab. Statistical analyses of slab dip data from a number of transects across different subduction zones [*Jarrard*, 1986; *Lallemand et al.*, 2005; *Cruciani et al.*, 2005] show a poor correlation between the angle of subduction and the age of the subducting lithosphere, A_{sub} (Figures 1a and 1b) indicating that there may be significant variation in the hydrodynamic torque or other factors, described above, masking the dependence on slab buoyancy.

[8] In order to attempt to unmask the slab buoyancy dependence of slab dip, we present slab dip data for which, following *Lallemand et al.* [2005], we have removed data from transects where slab dip is likely affected by other factors (Figures 1c and 1d; where 56 and 45 transects were removed from Figures 1a and 1b, respectively). We have removed data from near-edge transects as they may be affected by the toroidal flow around the slab edges [*Royden and Husson*, 2006; *Piromallo et al.*, 2006; *Schellart et al.*, 2007; *Di Giuseppe et al.*, 2008] and data from slabs that have reached the lower mantle, because the angle of subduction can change due to the viscosity increase in the lower mantle [e.g., *Billen and Hirth*, 2007]. As shown in Figures 1c and 1d, the correlation between slab dip and subducting plate age clearly improves when removing these data, but we can still find "anomalous" data, such as high slab dips in transects across the Central America subduction zone, where the young Cocos plate subducts steeply. Thus it is important to identify, analyze and isolate the other potential factors that might affect slab dip in order to evaluate their relative roles. Therefore, we study not only the influence of the thermal state of the subducting plate, but also that of the overriding plate, which is expected to influence the hydrodynamic torque exerted on the slab through the variation in viscosity of the mantle wedge (i.e., equation (5)). The influence of the nature, continental or oceanic, of the overriding plate is supported by observational evidence showing that subduction beneath oceanic plates is steeper than under continental plates [*Uyeda and Kanamori*, 1979; *Jarrard*, 1986; *Lallemand et al.*, 2005]. However, caution must be taken as it is hard to separate this correlation from the possible effect of slab polarity (most of the eastward dipping slabs are overridden by continental plates, whereas most westward dipping slabs subduct under oceanic plates), as pointed out by *King* [2001]. *Lallemand et al.* [2005] found that the mean slab dip at depths greater that 125 km is of 70° ± 11° for oceanic overriding plates but only 53° ± 12° for continental upper plates. This difference in slab dip is likely related to the different viscosity structure under each type of overriding plate indicating a dependence on the hydrodynamic torque. Similarly, *Pérez-Gussinyé et al.* [2008] find that slabs close to areas of high elastic thickness in the overriding plate have shallower dips, and suggest that the viscosity structure under the overriding plate has a significant influence on the occurrence of flat subduction.

[9] A number of studies have explored the influence of the viscosity structure of the slab and surrounding mantle on the dynamics of subduction (see *King* [2007] and *Billen* [2008] for extensive reviews). For example, *van Hunen et al.* [2002a, 2002b, 2004, and references therein] explored the influence of the relative velocity of the overriding plate, slab buoyancy and rheological parameters. *Čížková et al.* [2002] showed that the slab strength modulated the effects of trench retreat on deep slab dip. *Billen and Hirth* [2005, 2007] carried out a systematic study of the influence of rheology, slab's strength, mantle viscosity and the age of the subducting plate on subduction dynamics. The effect of the structure of the overriding lithosphere and the mantle wedge has been studied in terms of the presence of hydrous materials in the mantle wedge [e.g., *Manea and Gurnis*, 2007; *Arcay et al.*, 2008] or the presence of continental roots [*O'Driscoll et al.*, 2009]. *Eberle et al.* [2002] investigated the effect of the boundary condition on the upper plate (fixed versus free slip) on the thermal and viscosity structure in the mantle wedge. *Roda et al.* [2011] investigated the influence of the thickness of an overriding continental plate on slab dip, and found that it decreases with the increase in the upper plate thickness.

[10] In this study we hypothesize that some of the observed variability in slab dynamics and geometry may be controlled by the variation in the thermal state of the overriding plate. To quantitatively test this hypothesis, we investigate the influence of the thermal state of both overriding and subducting plates on slab dip using 2-D thermomechanical models for an ocean-ocean subduction system where subduction is driven by means of a kinematic boundary condition. We note that while the modeling setup and rheology used in this study is similar to the study by *Billen and Hirth* [2007], in contrast with their models, which did not consider the effect of the overriding plate and obtained significant slab dip variations only after the slab was partially supported by the high lower-mantle viscosity, we focus here on

shallow mantle processes controlling slab dip and subduction style.

2. Methodology

2.1. Governing Equations and Numerical Method

[11] The model domain represents a vertical section running parallel to the subduction direction, in which equations of conservation of mass, momentum and energy (equations (6), (7), and (8), respectively) are solved for an incompressible 2-D fluid with high Prandtl number, which allows us to neglect inertial forces on the momentum equation:

$$\nabla \cdot \vec{u} = 0 \tag{6}$$

$$\nabla \cdot \left[\eta\left(\nabla\vec{u} + (\nabla\vec{u})^T\right)\right] - \nabla P + \rho\vec{g} = 0 \tag{7}$$

$$\rho C_p\left(\frac{\partial T}{\partial t} + \vec{u}\cdot\nabla T\right) = k\nabla^2 T + Q_{ad} \tag{8}$$

where ρ is the density $\vec{u}$ is the velocity field, η is the viscosity, the term multiplied by the viscosity is the strain rate tensor, P is the total pressure, C_p is the specific heat, k is the thermal conductivity and Q_{ad} is the adiabatic heating. The dot symbol · denotes the scalar product and the superscript T denotes transposition.

[12] Here we have considered only density variations due to temperature following the simplified state equation: $\rho = \rho_0[1 - \alpha(T - T_0)]$, where, ρ_0 is the density at T_0 = 273 K and α is the thermal expansion coefficient. In the present formulation of the energy equation (equation (8)) we neglect internal heat sources, shear heating and latent heat released during phase transformation, but we do take into account thermal effects due to pressure changes. Therefore, we calculate heat released/absorbed through adiabatic upwelling/downwelling using the expression $Q_{ad} = -\rho\alpha g v_y T$, where v_y is the vertical component of velocity. The reader is referred to *Ita and King* [1994] and *Schubert et al.* [2001] for derivation of this term from the primitive extended Boussinesq energy equation [*Oxburgh and Turcotte*, 1978, equation 4.3].

[13] These coupled equations ((6)–(8)) are solved using the finite element codes included in the software COMSOL Multiphysics 3.5a (Addlink Software). We have used the direct solver PARDISO [*Schenk and Gärtner*, 2004, 2006] included in the software, because it is faster and requires less memory than other solvers. The modeled section is discretized through a mesh of triangular elements whose density varies from one element every 2 km in the area of the plate boundary to one every 150 km in the lower mantle. For the momentum equation we used Lagrange P2-P1 elements, which are quadratic in velocity and linear in pressure. Lagrange Quadratic elements were used to model the temperature field.

2.2. Model Setup

[14] The modeled vertical section is 1200 km deep and it includes the lithosphere, sublithospheric upper mantle and a portion of the lower mantle (Figure 2a). The width of the modeled section changes from 3500 to 5500 km to control the age of the subducting plate (see section 2.3). In order to reproduce subduction, we have imposed a constant velocity u_s = 5 cm/yr at the upper boundary of the subducting plate, whereas the upper boundary of the overriding plate is fixed. This condition of a fixed overriding plate has been shown to be in better agreement than a free-slip condition with geophysical observations, as it leads to tectonic erosion of the lower lithosphere of the overriding plate causing high-temperatures, low seismic velocities, high attenuation and high heat flow beneath volcanic arc [*Eberle et al.*, 2002]. The plates are separated by a plate boundary modeled as a narrow low viscosity zone. A free slip boundary condition is applied to the bottom and side boundaries of the model domain. Our modeling is not able to properly simulate the dynamics of plate bending at the trench because vertical motion on the top surface is not allowed. While the surface boundary conditions may affect bending of an elastic slab at very shallow depths, because the slab is viscous it has no memory of how it deforms going into the trench nor is it able to transmit "bending" stresses downdip. Therefore, we consider that the surface boundary conditions cannot affect the deeper deformation of the slab.

[15] The imposed velocity condition on the top of the subducting plate is necessary to initiate subduction and facilitates controlling both the subduction velocity and the subducting plate age. However, it is a modeling tool and it is therefore important to be clear about what it represents and what influence it is expected to have on the subduction results.

[16] First, this boundary condition is used to account for convergence caused by the combination of forces driving subduction, but not included in the 2D cross section modeled here, without making any hypothesis about the relative importance of these forces.

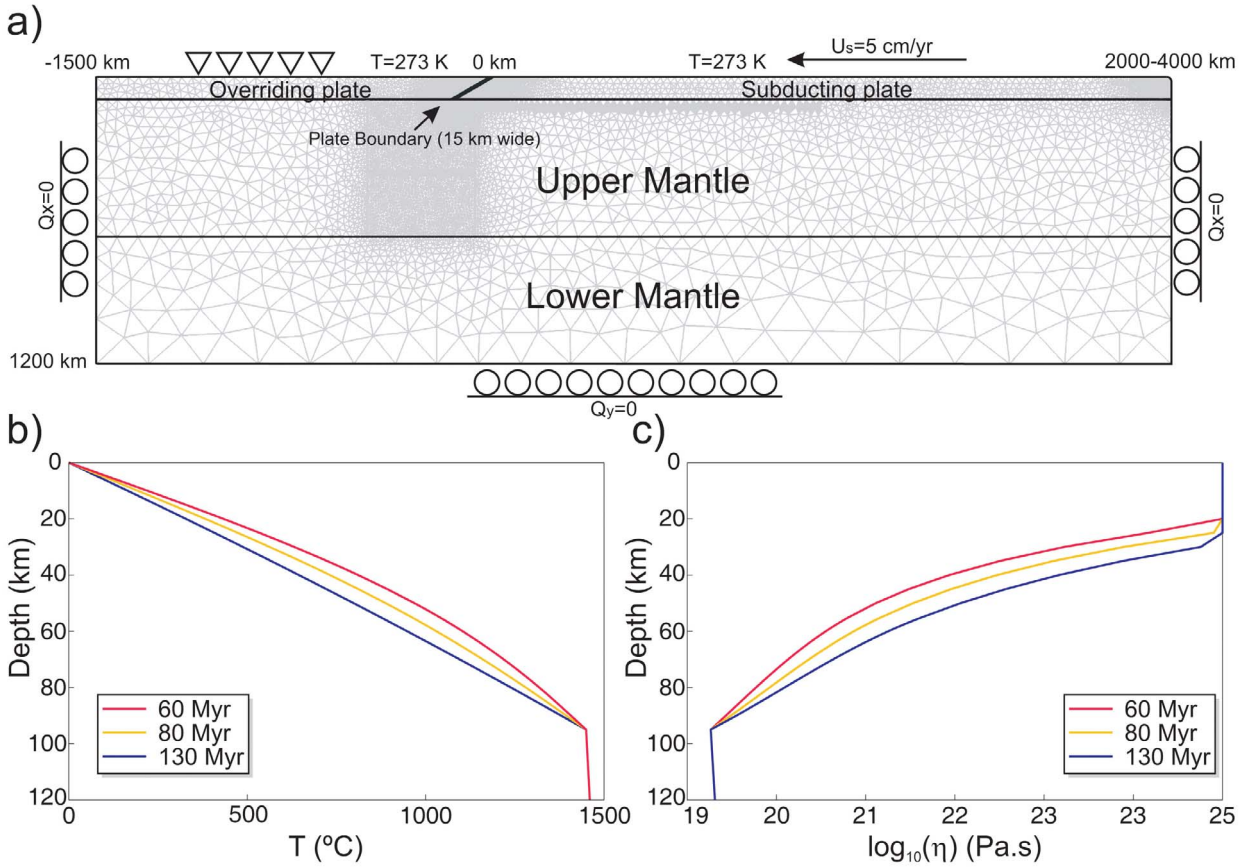

Figure 2. Model setup. (a) Schematic representation of the modeled 2D vertical cross section showing the finite element mesh and boundary conditions. Note the modeled domain width is varied from 3500 to 5500 km to allow for models with different, but constant subducting plate age at the plate boundary. (b) Initial temperature and (c) viscosity profiles for three different plate ages. A reference effective strain rate of 10^{-15} s^{-1} and a maximum viscosity cut-off of $\eta_{max} = 10^{25}$ Pa·s are assumed.

For example, *Conrad and Lithgow-Bertelloni* [2002, 2004] found that the velocities of the plates were best predicted when about half of the driving force came from net slab pull (balance between slab pull and subduction resistance) and half came from slab suction and distributed basal tractions due to the convection which the slabs (even detached) induce in the lower mantle. Moreover, even if subduction was entirely driven by the negative buoyancy of the full (3D) slab, locally the slab dynamics may be affected by regional features such as the presence of buoyant oceanic plateaus [e.g., *van Hunen et al.*, 2002a, 2002b, 2004] or changes in the thermal state of the overriding plate, as will be investigated here. Therefore, the negative buoyancy of the full slab could continue to pull the slab down even if locally other forces resist subduction and the 2D section of the slab is unable to fully drive subduction.

[17] Second, previous studies show that for weak to moderately strong slabs, the evolution of the slab in the mantle is not controlled by the kinematic boundary condition [*Han and Gurnis*, 1999]. Similarly, *Billen and Hirth* [2007] showed that with the type of rheology being used, most of the work done by the boundary condition is dissipated within the subducting plate and bending region and therefore the slab dynamics in the mantle is free to evolve in response to the local forces.

[18] Therefore, while the kinematic boundary condition on the subducting plate is not ideal, nor realistic, it facilitates incorporating the net effect of large-scale mantle flow and out-of-cross-section (3D) plate driving forces with confidence that the boundary condition does not itself control the evolution of the subducting slab.

2.3. Initial Thermal Structure

[19] The temperature distribution in the lithosphere is defined by the plate cooling model (first described

Table 1. Model Parameters

Symbol	Meaning	Value	
u_s	Subduction velocity	5 cm yr^{-1}	
W	Domain horizontal extent	3500 to 5500 km	
H	Domain vertical extent	1200 km	
L	Lithospheric thickness	95 km	
T_L	Temperature at the base of the lithosphere	1723 K	
K	Thermal conductivity[a]	3.2 W m^{-1} K^{-1}	
A	Thermal expansion coefficient[b]	3.7×10^{-5} K^{-1}	
C_p	Specific heat[a]	1.3×10^{3} J K^{-1} kg^{-1}	
ρ_0	Reference density (at 273 K)[b]	3400 kg m^{-3}	
E	Shear zone width/dip	15 km/30°	
η_b	Maximum viscosity at the shear zone	$10^{21} - 3 \times 10^{22}$ Pa s	
η_{max}	Maximum viscosity	$10^{24} - 10^{25}$ Pa s	
Symbol	Rheological Parameters[c]	Diffusion	Dislocation
n	Stress exponent	1	3.5
A	Preexponential factor (Pa)	1	$90{\cdot}10^{-21}$
	Activation energy (J/mol)	335000	480000
V	Activation volume (m^3/mol)	$4.0{\cdot}10^{-6}$	$11.0{\cdot}10^{-6}$
d	Grain size (m)	10^{-2}	
p	Grain size exponent	3.0	
C_{OH}	OH concentration (ppm-H/Si)	1000/1	1000/1
r	C_{OH} exponent	1.0	1.2

[a] *Schubert et al.* [2001].
[b] *Schmeling et al.* [1999].
[c] *Hirth and Kohlstedt* [2003].

by *McKenzie* [1967]). This thermal model for the oceanic lithosphere assumes that the temperature is kept constant at the surface and at a given depth L, which defines the plate thickness. This 'plate thickness' is often referred to as the asymptotic (in the limit of very old lithosphere) lithospheric thickness. The plate cools down from an initial (at the ridge) temperature uniform across the plate thickness, and therefore its thermal state is controlled by its age. We use the solution for temperature distribution (assuming a surface temperature of 0°C) given by *Carslaw and Jaeger* [1984].

$$T_{lit}(y,t') = T_L\left[\frac{y}{L} + \sum_{n=1}^{\infty}\frac{2}{n\pi}\sin\left(\frac{n\pi y}{L}\right)\exp\left(-\frac{n^2\pi^2 kt'}{\rho C_p L}\right)\right] \quad (9)$$

where T_L is the temperature at the base of the plate ($y = L$) and at the ridge, L is the plate thickness and t' is the age of the lithosphere (parameters listed in Table 1). We have adopted the values T_L = 1450°C and L = 95 km, from plate model GDH1 [*Stein and Stein*, 1992]. In contrast with *Roda el al.* [2011], who modified the thermal state of both plates only by changing their thicknesses, our choice of the plate cooling model requires that the plate thickness is kept constant while the thermal state is modified by varying the lithospheric age (Figure 2b). Therefore, an advantage of using a plate model is that it allows us to isolate the temperature effects, as the plate thickness is held constant. The age of the subducting plate increases with the distance from the right boundary, which represents an oceanic ridge. Models are designed to keep a constant subducting plate age in order to analyze the effects of plate age without other complications. The age of the subducting lithosphere at the plate boundary is computed as $t' = D_r/u_s$, where D_r is the distance from the plate boundary to the right model boundary, Therefore, as the subduction velocity u_s = 5 cm/yr is maintained constant in all the models, D_r is changed from one model to another to modify the age of the subducting lithosphere at the plate boundary. Accordingly, the width of the modeled section is varied between 3500 and 5500 km to change the age of the subducting plate at the plate boundary from 40 to 80 Myr, respectively. For simplicity, the crust is not included in either plate and a uniform age is used for overriding plate (except for Models F and G, see Table 2).

[20] Beneath the lithospheric plate, we impose an adiabatic distribution for the mantle temperature:

$$T_m(y) = T_L\exp\left(\frac{g\alpha}{C_p}(y - L)\right) \quad (10)$$

The bottom and side boundaries are thermally insulated and the upper boundary is set to a fixed temperature of 273 K for both plates.

Table 2. Parameters for All of the Models Completed for This Study

Model	A_{ov} (Myr)	A_{sub} (Myr)	η_{max} (Pa·s)	η_b (Pa·s)	u_s (cm/yr)	Subduction Style
A	60	50	10^{25}	$3{\cdot}10^{22}$	5.0	Reference model
B	60	70	"	"	"	High angle subduction
C	130	70	"	"	"	Low angle subduction
D	80	50	"	"	"	Flat subduction
E	60	40	"	"	"	Coupled
F	150/80	50	"	"	"	Coupled
G	40/60	40	"	"	"	Flat subduction
H	80	40	10^{24}	10^{21}		Coupled
I	30	40	10^{24}	10^{21}	"	High angle subduction
J	200	50	10^{24}	10^{21}	"	Flat subduction
K	80	50	10^{25}	$3{\cdot}10^{22}$	7.5	High angle subduction
L	60	40	"	"	7.5	Intermediate angle
M	60	70	"	"	2.5	Low angle subduction
N	130	70	"	"	2.5	Coupled

2.4. Rheology

[21] In the mantle, deformation is thought to be accommodated by two different mechanisms: diffusion creep (*df*) and dislocation creep (*dis*). For olivine, diffusion creep has a linear relationship between stress and strain rate, whereas dislocation creep has a power law stress-strain rate relationship or a viscosity that depends on the effective strain rate, $\dot{\varepsilon}_E = \left(\frac{1}{2}\dot{\varepsilon}_{ij}\dot{\varepsilon}_{ij}\right)^{1/2}$. Here we use a composite rheology for which the total strain rate is given by the sum of the strain rate accommodated by diffusion creep and the strain rate accommodated by dislocation creep at the same stress. This results in the composite viscosity given by

$$\eta_{comp} = \frac{\eta_{df}\eta_{dis}}{\eta_{df} + \eta_{dis}} \tag{11}$$

where η_{df} and η_{dis} represent diffusion and dislocation viscosities. Both viscosities can be expressed in the same form [*Hirth and Kohlstedt*, 2003]:

$$\eta_{df,dis} = \left(\frac{d^p}{AC_{OH}^r}\right)^{\frac{1}{n}} \dot{\varepsilon}_E^{\frac{1-n}{n}} \exp\left(\frac{E + P_{lit}V}{nRT}\right) \tag{12}$$

where d is the grain size, p is the grain size exponent, A is the pre-exponential factor, C_{OH} is OH concentration, E and V are activation energy and volume, P_{lit} is the lithostatic pressure, R is the gas constant, and n is the stress exponent (Table 1). Therefore, for the diffusion viscosity (n = 1; p = 3) there is no dependence on the strain rate, while for the dislocation viscosity (n = 3.5; p = 1) the viscosity is non-Newtonian with a viscosity that decreases with increasing strain rate by means of a power law. In addition, we have imposed a maximum viscosity cut-off, $\eta_{max} = 10^{25}$ Pa·s, for cold temperatures in which the viscosity laws given here are no longer applicable, but we do not impose a minimum viscosity cut-off. Figure 2c shows initial viscosity profiles over the range of ages used and assuming a strain rate of 10^{-15} s^{-1}.

[22] While our models do not include plastic yielding (but strength is limited by a maximum viscosity cut-off), previous models [*Billen and Hirth*, 2007; *Faccenda et al.*, 2009] have shown that the slab yields throughout its thickness as it enters the trench: once the material has yielded it no longer has any elastic strength. Therefore elasticity is neglected in this study, as we focus on deeper plate deformation processes.

[23] We have also imposed a narrow low viscosity region at the plate boundary. This low viscosity channel is intended to simulate a fault that decouples both plates without producing singularities on the stress distribution [*Billen and Hirth*, 2007; *Kukačka and Matyska*, 2004]. Viscosity, geometry, depth and width of this weak region have great influence on the dynamics of subduction [*Jischke*, 1975; *Kincaid and Sacks*, 1997; *Chen and King*, 1998; *Manea and Gurnis*, 2007; *Burkett and Billen*, 2009; *De Franco et al.*, 2007]. In the reference model the low viscosity channel is 15 km wide and 95 km deep and with a maximum allowed viscosity of $\eta_b = 3{\cdot}10^{22}$ Pa s. Results of tests with different values of this maximum viscosity cut-off are reported in the discussion section. Viscosity in this shear zone actually can be lower than this upper bound as a result of the applied temperature and stress-dependent rheology. The shear zone depth is chosen to reach the base of the overriding plate such that the subducting plate can slide uniformly along the boundary. A shorter shear zone leads to strong viscous coupling between the sub-

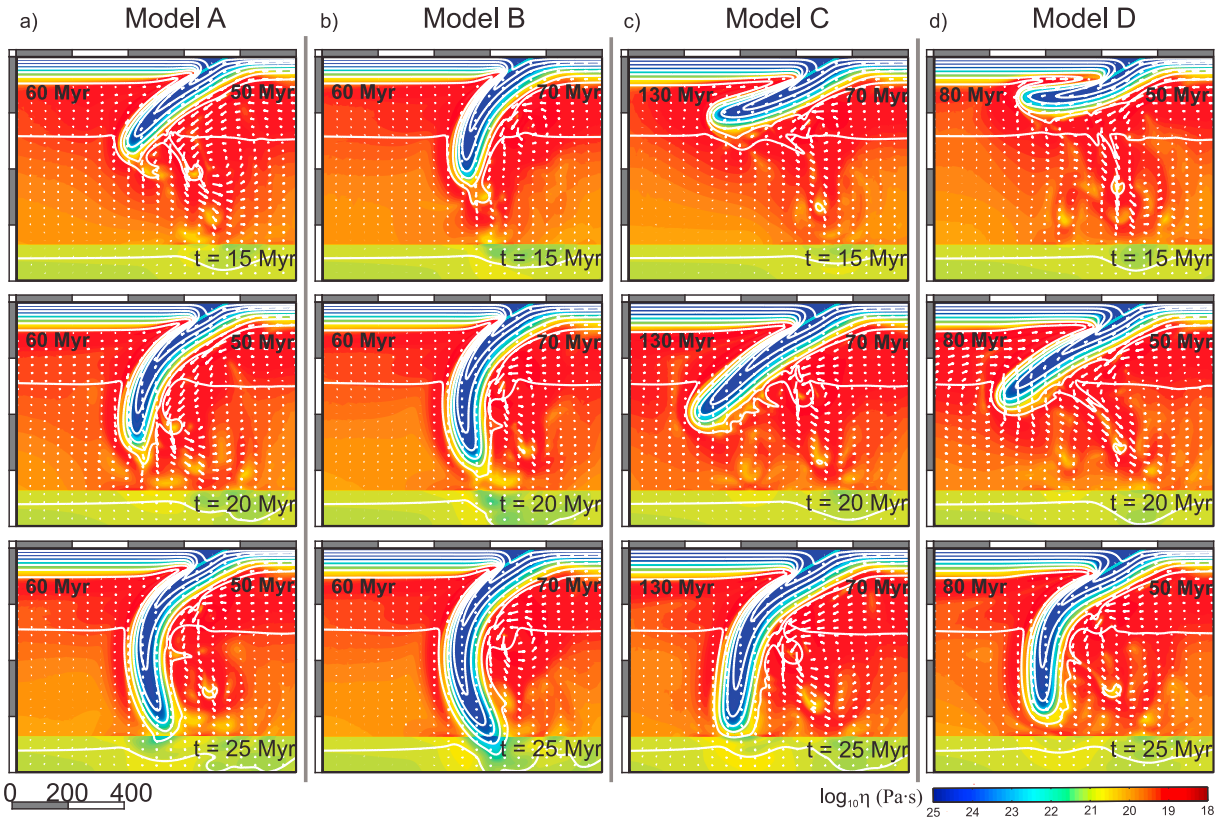

Figure 3. Model results at three different evolution times for different ages of the overriding and subducting plates. The four different simulations are examples of different styles of subduction: (a) reference model (A: overriding plate of 60 Myr and subducting plate of 50 Myr), (b) high-angle subduction (B: overriding plate of 60 Myr and subducting plate of 70 Myr), (c) low-angle subduction (C: overriding plate of 130 Myr and subducting plate of 70 Myr) and (d) flat subduction (D: overriding plate of 80 Myr and subducting plate of 50 Myr). Decimal logarithm of the viscosity (color), isotherms every 200 K (contour) and velocity field (arrows) are shown. Subducting plate moves at 5 cm/yr.

ducting and overriding plate, which prevents subduction. A constant dip of 30° is imposed, which is consistent with the mean value of slab dip at shallow depths (32° ± 11°) obtained by *Lallemand et al.* [2005].

[24] Including a low strength crust on the subducting plate would eliminate the need to impose a fixed low viscosity zone as it would feed dynamically the low viscosity region at the plate boundary. This would allow the interplate contact to react dynamically and adjust its dip and position. However, we have preferred to fix the trench with an imposed weak channel because it allows the effect of the overriding plate thermal structure and mantle wedge dynamics to be isolated from other effects.

3. Results

[25] Here we present the results of a suite of models designed to determine the relative importance of the thermal state of the overriding and subducting plates in controlling the slab dip. We have also tested the effect of the viscosity at the plate boundary and of maximum overall viscosity. Table 2 lists the parameters for all of the 31 models completed for this study, while the time snap-shots of models with letters A–F are shown in Figure 3. The angle of subduction that results in the models varies significantly with depth, so we present the results in two different depth ranges: α_s is the mean shallow angle, measured between 100 and 200 km, and α_d is the mean deep angle measured between 300 and 400 km. The mean angle in each depth interval is computed automatically using tracers located at the surface of the slab.

[26] In order to facilitate the interpretation of the results, we have computed the gravitational and suction torques exerted by a rigid (but curved) slab having the geometry obtained at each time step. We have used equations (1) and (2), which require the

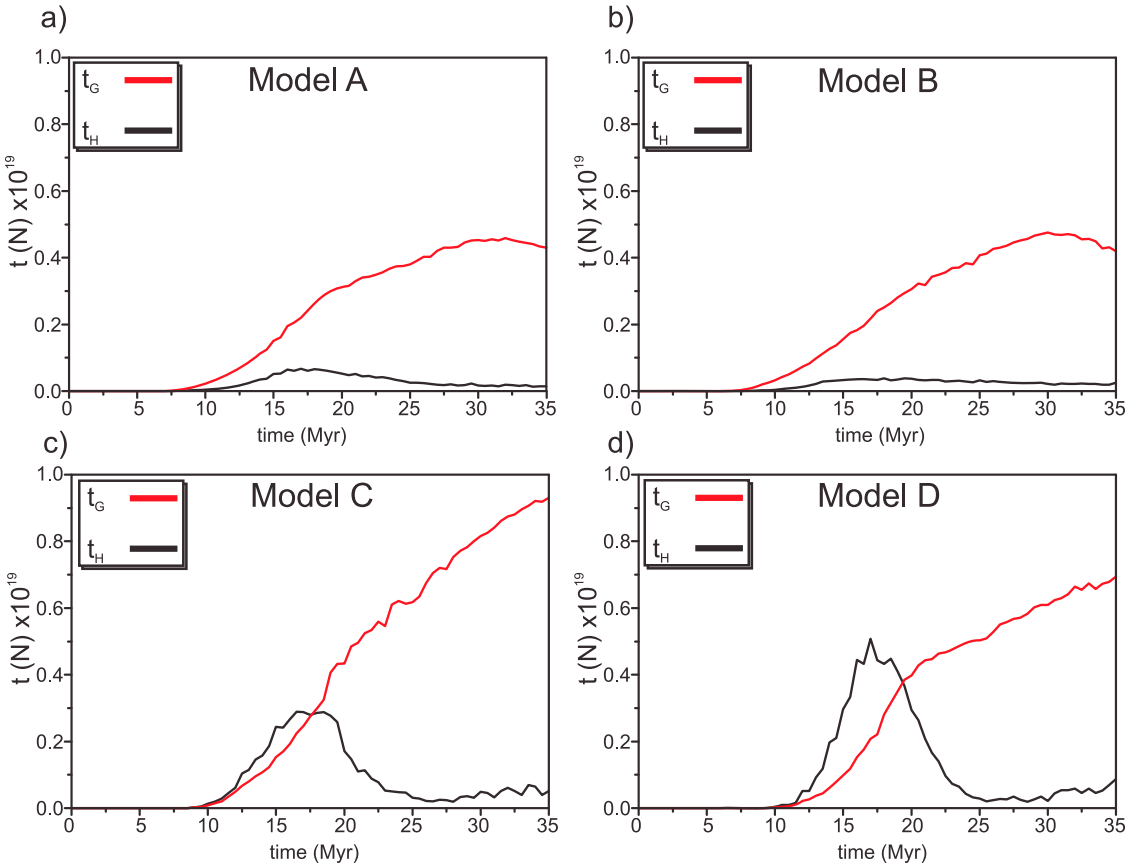

Figure 4. Time evolution of the gravitational (red) and hydrodynamic (black) torques per unit slab width for the four models shown in Figure 3.

calculation of the density contrast and the dynamic pressure. We have computed the dynamic pressure (hereafter, referred to as the pressure) 10 km above the slab (defined by tracers), and have neglected the contribution of the pressure beneath the slab as we obtain that it is much lower than the pressure above it. We have also neglected the pressure contribution below 300 km depth as pressure is expected to tend to zero with depth for slab-induced corner flow. It is important to keep in mind that the modeled slab is viscous and bends in response to the local torque balance, therefore actual torques are not uniformly affecting the entire slab, but the gravitational torque has more effect in the deeper portion of the slab while the suction torque mainly affects the shallow portion, resulting in a variable dip along the slab.

3.1. Reference Model

[27] The reference model established for comparison purposes (model A; Figures 3a and 4a and Animation S1 in the auxiliary material) includes an overriding plate of 60 Myr and a subducting plate of 50 Myr.[1] At the beginning of the simulation the subducting plate bends and penetrates into the mantle. As the slab reaches greater depths, the gravitational torque increases (Figure 4a), and the subduction angle also increases. The gravitational torque tends to stabilize with time due to the competing effects of increasing slab length and dip (equation (1)) and after an evolution of around 25 Myr the slab reaches a steady state and the angle of subduction remains almost constant. No substantial variation of the subduction angle occurs as the slab sinks into the lower mantle, provided that the viscosity contrast between the upper and the lower mantle is of only one order of magnitude. At times greater than 35 Myr of evolution (not shown), the slab approaches the base of the modeled domain and the results are no longer realistic.

[28] The viscosity on the surface of the slab is low due to the high strain rate. This reduced viscosity causes a decrease of the hydrodynamic torque and a

[1]Auxiliary materials are available in the HTML. doi:10.1029/2011GC003859.

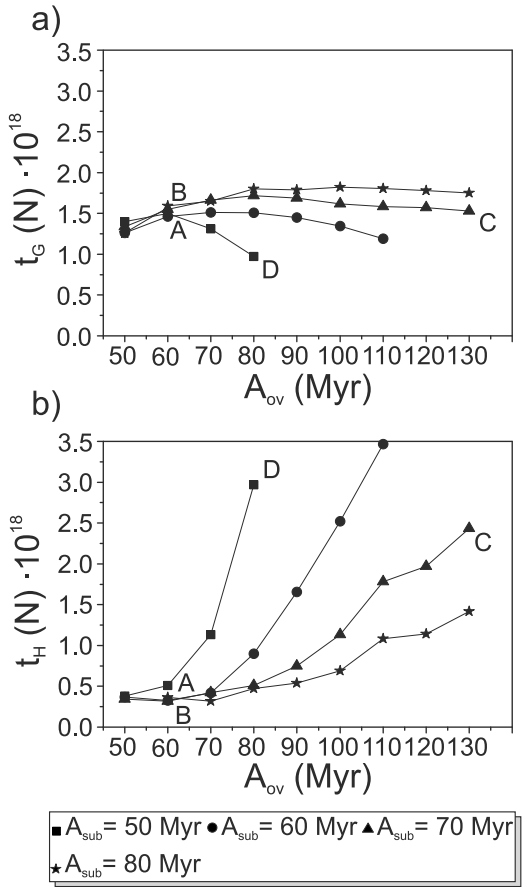

Figure 5. (a) Gravitational and (b) hydrodynamic torques per unit slab width as a function of the age of the overriding plate for different ages of the subducting plate, after 15 Myr of evolution. Capital letters in the figures indicate Models A–D shown in Figure 3 and Table 2.

higher angle of subduction compared to simulations with Newtonian rheology [*Billen and Hirth*, 2005].

3.2. Influence of Thermal State of the Subducting Plate

[29] We start by varying the age of the subducting plate (by changing the distance from the plate boundary to the ridge, D_r) in order to control its thermal state. During the first 15 Myr of evolution, the influence of the thermal state of the subducting plate is significant. As expected, the gravitational torque is slightly higher for older subducting plates (Figure 5a), which in turn causes older plates to subduct with higher angles (Figures 3a, 3b, and 6a). Slab dip variability with the age of the subducting plate is more significant for older overriding plates. For example, at times less than 15 Myr, for an overriding plate of 80 Myr, simulations predict an increase of shallow slab dip from ~5° (flat) for a 50 Myr subducting plate age to a dip as high as ~45° for an subducting plate age of 80 Myr (Figure 6a). In contrast, there is almost no variation in slab dip with subducting plate age for an overriding plate of 50 Myr (Figure 6a). This effect can be understood as resulting from the greater sensitivity of the gravitational torque to the slab buoyancy for smaller angles (equation (1) and Figure 5a), which are only achieved for old overriding plates, as explained below.

[30] For all the models tested, by 25 Myr, the slab dip increases and the initial differences in slab dip caused by variation in subducting plate age have decreased dramatically (Figures 6c and 6d). This evolution to a steep slab steady state occurs because as the slab lengthens and the negative buoyancy of the slab increases, the gravitational torque becomes significantly larger than the hydrodynamic torque for all the models (Figure 4b). However, the hydrodynamic suction is greater for lower slab dips (equation (5)) and therefore young plates subducting with shallow dips cause suction torques that are higher than older plates (Figure 5b). At this steady state stage, the thermal state of the subducting plate has little influence on the dip angle at the shallowest portion of the slab (Figure 6b): the angle for the deeper portion of the slab does slightly decreases (Figure 6c) because older plates are more viscous and resist bending. Therefore, the expected loss of sensitivity of slab dip to subducting plate age for long-term subduction should be taken into account when statistically analyzing slab dip data.

3.3. Influence of Thermal State of the Overriding Plate

[31] To test the influence of the thermal state of the overriding plate we vary the plate age to control its thermal state.

[32] As expected from consideration of the hydrodynamic forces, subduction under an older plate results in a higher suction torque around 15–20 Myr (Figures 4c, 4d, and 5b), which leads to a lower slab dip than subduction under a younger plate (Figure 3b versus Figure 3c and Figure 3a versus Figure 3d). For young (or hot) overriding plates the viscosity in the deeper part of the lithosphere is relatively low, thus allowing for the thermal erosion of the base of the lithosphere close to the plate boundary. This thermal erosion allows the high strain rate mantle wedge flow to migrate into the shallower regions of the wedge corner, further reducing the viscosity; so the mantle wedge expands into the lithosphere, dramatically reducing the suction torque.

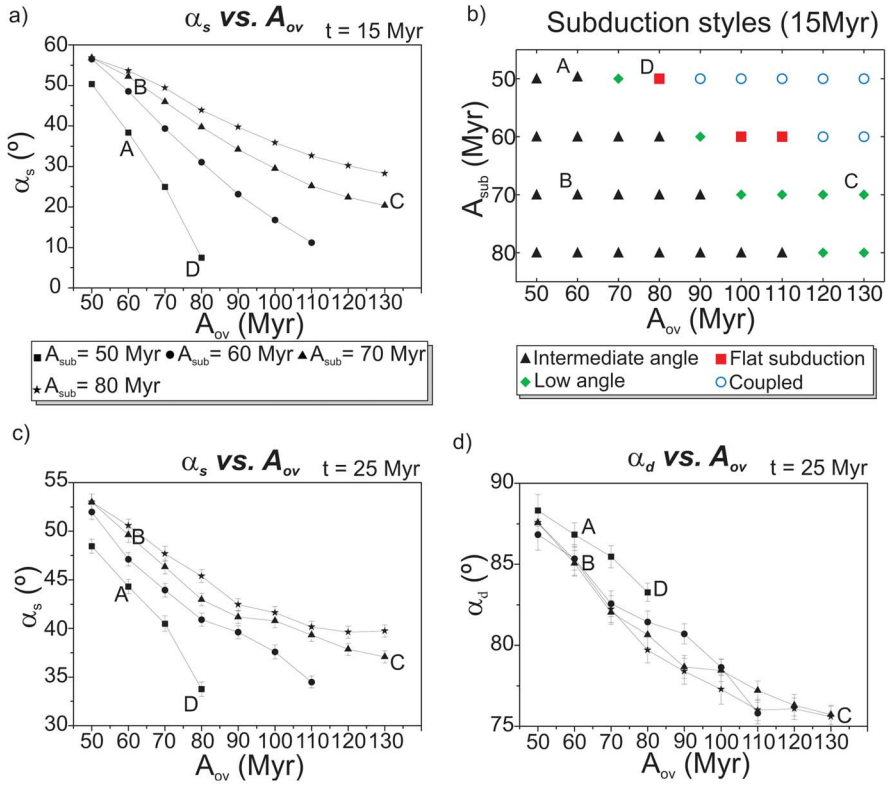

Figure 6. Mean slab dip as a function of the age of the overriding plate for different ages of the subducting plate measured (a) between 100 and 200 km depths (α_s) after 15 Myr of evolution. (b) Distribution of subduction styles depending on the age of the overriding a subducting plates after 15 Myr. (c) Slab dip α_s measured at depths between 100 and 200 km and (d) slab dip α_d measured at depths between 300 an 400 km, after 25 Myr. Capital letters in the figures indicate Models A–D shown in Figure 3 and Table 2.

[33] For a subducting plate age of 60 Myr, by 15 Myr of evolution we obtain a shallow slab dip decrease of about 50° and an increase of the suction torque per slab width of about $3{\cdot}10^{18}$ N, going from a model with an overriding plate age of 50 Myr to a model with an overriding plate age of 110 Myr (solid circles in Figures 5a and 6a). The influence of the thermal state of the overriding plate becomes more significant for young subducting plates, as they are less viscous and therefore easier to deform (both by bending and unbending) in response to the net torque. Moreover, as the resulting slab dip is lower for younger subducting plates, the hydrodynamic suction in the mantle wedge increases (equation (5)), leading to high variations of the suction torque with the age of the overriding plate (Figure 5b).

[34] After 25 Myr, the influence of the thermal state of the overriding plate diminishes as the hydrodynamic torques from all models are similar (Figure 4), but the simulations still produce a maximum difference of almost 20° for the shallowest part of the slab, α_s (Figure 6c) and 15° for the deepest region, α_d (Figure 6d) as a function of overriding plate age. The effect of the age of the overriding plate in the shallow slab dip α_s is again more significant for young subducting plates. In contrast, between 300 and 400 km depth, the slab dip α_d is almost independent of its age. Not only are the differences in slab dip caused by different subducting plate ages negligible, but we also find that the amount that the slab dip decreases for a given increase in the age of the overriding plate is almost identical for all subducting plate ages, about 0.25°/Myr (Figure 6d).

[35] All the simulations presented here show that the influence of the age of the overriding plate is always more important than the effect of the age of the subducting plate. After 15 Myr of evolution, increasing the subducting plate age from 50 Myr to 80 Myr leads to increases of α_s ranging from 6° (for A_{ov} = 50 Myr in Figure 6a) to 36° (for A_{ov} = 80 Myr in Figure 6a), whereas if the age of the overriding plate varies from 50 Myr to 80 Myr, the decreases of α_s range from 13° (A_{sub} = 80 Myr in Figure 6a) to 45° (A_{sub} = 50 Myr in Figure 6a). After 25 Myr of evolution, this trend is maintained but with much smaller variations in slab dip. This

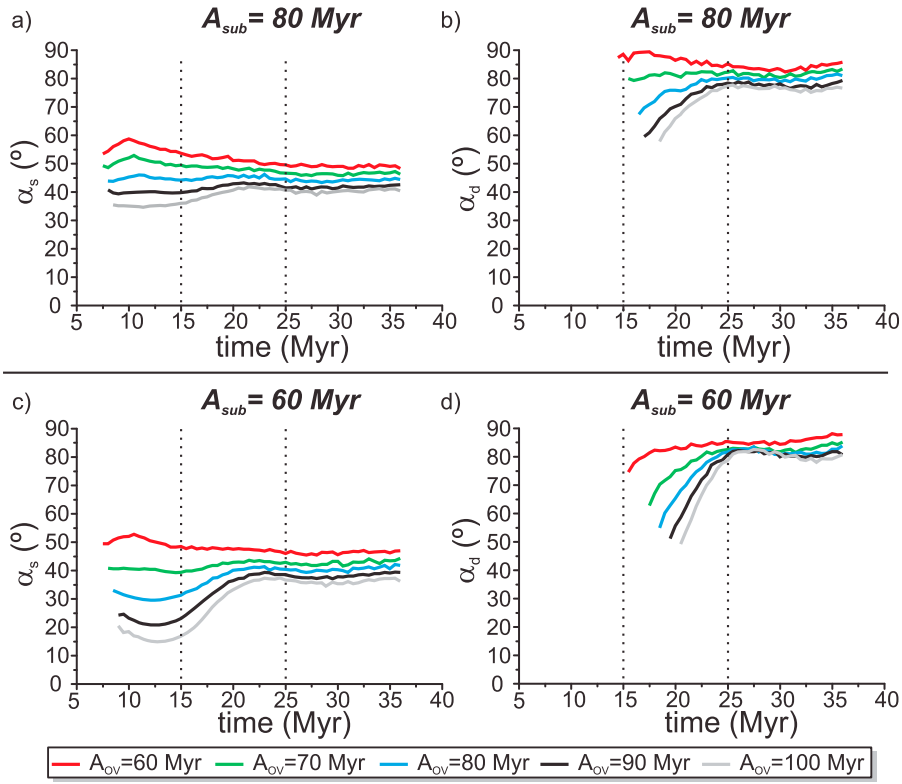

Figure 7. (a, b) Time evolution of the mean slab dip measured between 100 and 200 km (α_s) and (c, d) between 300 and 400 km depth (α_d). Comparison of the evolution for different overriding plate age at a constant subducting plate age of 80 Myr (Figures 7a and 7b) and 60 Myr (Figures 7c and 7d). Colors indicate different ages of the overriding plates, as described in the legend.

result highlights the importance of discriminating between different overriding plate thermal states in statistical analysis of slab dip data, to prevent this effect masking that of the slab age. The gravitational torque is less sensitive to variations of either plate's age compared to the hydrodynamic torque (Figure 5a versus Figure 5b), and for this reason there is less variability of α_d (mainly controlled by the gravitational torque) than of α_s with plate age.

[36] Although we model an ocean-ocean subduction system, we consider that the qualitative results are also valid for the case of an overriding continental plate. We therefore assume (also on the basis of sensitivity tests to variations in plate thickness) that a thick overriding plate can be approximated as a cold plate with an older age, which creates a thicker region of high viscosity at the base of the lithosphere. However, caution must be taken with this approximation, as radiogenic heat production must be taken into account for continental lithosphere.

3.4. Subduction Styles

[37] Depending on the age of the overriding and subducting plates, the simulations performed in this study show different evolution of the slabs, resulting in different subduction styles (mapped in the diagram shown in Figure 6b).

3.4.1. High Angle Subduction

[38] For old subducting plates (Model B; Figures 3b, 7a, and 7b and Animation S2) and, or young overriding plates (red and green lines in Figures 7c and 7d) the gravitational torque is always higher than the suction torque (Figure 4b) and therefore the initial slab dip is high. For the youngest overriding plates and the oldest subducting plates (red lines in Figures 7a and 7b) the slab dip decreases slightly with time, around 10°. The slab flattening is caused by the increase of the suction of the shallower portion of the slab due to the cooling of the material in the mantle wedge.

3.4.2. Low Angle and Flat Subduction

[39] Simulations with young subducting plates and old overriding plates tend to reproduce low slab dips (Model C; Figure 3c and Animation S3). In contrast with the models that present high angle

subduction, at the beginning of the simulation the suction torque is higher than the gravitational torque (Figures 4c and 4d). As the simulation evolves and the slab length increases, the gravitational torque also increases. This causes the slab dip to increase, and consequently the suction torque decreases. Therefore, these simulations (blue, black and gray lines in Figures 7c and 7d) show that this low angle subduction style is transient and slab dip (along both depth ranges) increases significantly from 15 to 25 Myr of evolution, while the slab is sinking and lengthening in the upper mantle and the subduction style evolves to intermediate angle (at a depth range 100–200 km) and high angle (depths 300–400 km) subduction. At about 25 Myr, the torque balance reaches steady state and the slab dip remains nearly constant during the rest of the modeled evolution.

[40] For the youngest subducting plates and old overriding plates (Model D; Figures 3d and 4d and Animation S4) not only is the angle of subduction very low, but the slab reverses its curvature to flatten at ~100 km depth and advances sub-horizontally for hundreds of kilometers, due to the fact that during the early stages of evolution the suction torque is much higher than the gravitational torque (Figure 4d). A thin layer of low viscosity develops between the overriding and the subducting plates, which is maintained by the high strain rate between them and the nonlinear rheology. This layer decouples the plates from one another allowing for the formation of long segments of flat subduction. It is worthwhile remarking that we have been able to produce these long segments of flat subduction without imposing either a trenchward velocity of the overriding plate or density anomalies on the subducting plate. These results are in very good agreement with those found by *Roda et al.* [2011]. Taking into account that the model set-up, thermal and rheological structures assumed in both studies are substantially different, the consistency in qualitative results strengthens the robustness of the conclusion about the important role played by the overriding plate on controlling slab dip.

[41] After the formation of long flat segments, the evolution of slabs can follow two different paths. If the increase of the gravitational torque is high enough, the slab overcomes the suction torque and peels away from the overriding plate, increasing its angle, but it still remains relatively shallow-dipping for the shallowest portion of the slab (Model D; Figure 3d, gray line in Figure 7c, Figure 8a and Animation S4). The lower slab dip causes the suction torque to be higher than in other models with younger overriding plates, thus, the gravitational torque overcomes the suction torque in a later stage (Figure 4d versus Figure 4c), slightly delaying the sudden increase of the subduction angle. On the other hand, if the hydrodynamic torque always overcomes the gravitational torque, the low viscosity channel of the plate boundary closes up, coupling both plates and the results are no longer realistic (Model E; Figure 8c and Animation S5; A_{sub} = 40 Myr and A_{ov} = 60 Myr). This subduction style was named "coupled" by *Billen and Hirth* [2005] and occurred only in their models with Newtonian rheology and an old (80 Myr) overriding plate (although they did not consider variations in the overriding plate age).

[42] Our results do not necessarily imply that long-living flat subduction is not possible but, with the particular setup used here (fixed trench, absence of anomalously buoyant subducting material), when the hydrodynamic suction is strong enough to produce a flat slab segment, it occurs that both plates end up being coupled. Therefore, with this model setup, an additional mechanism to maintain the plates decoupled even for strong hydrodynamic suction (e.g., dehydration, melting processes, a low viscosity layer representing oceanic crust) is required to obtain non coupled flat subduction over longer periods of time. Including a low viscosity crust in the subducting plate would avoid this coupling, but as discussed before it would introduce a complexity (overriding plate and trench motion) that prevents the effect of thermal state of both plates from being isolated.

3.4.3. Laterally Varying Overriding Plate Age

[43] As a final test case, we consider the effect of laterally varying age of the overriding plate with distance from the trench (Figure 8). Model F has a subducting plate 50 Myr old and an overriding plate 80 Myr (from 0 to 200 km to the trench) that increases its age to 150 Myr (>200 km from the trench). This model can be compared with Model D (A_{sub} = 50 Myr and A_{ov} = 80 Myr; Animation S4). While Model D presented flat subduction (see section 3.4.2), in this case, when the slab reaches the older portion of the overriding plate, the hydrodynamic suction increases and both plates end up coupled (Figures 8a and 8b).

[44] On the contrary, the overriding plate in Model G becomes younger 200 km from the trench and its age decreases from 60 Myr (0–200 km from the trench) to 40 Myr (>200 km from the trench). This model can be compared with Model E (A_{sub} =

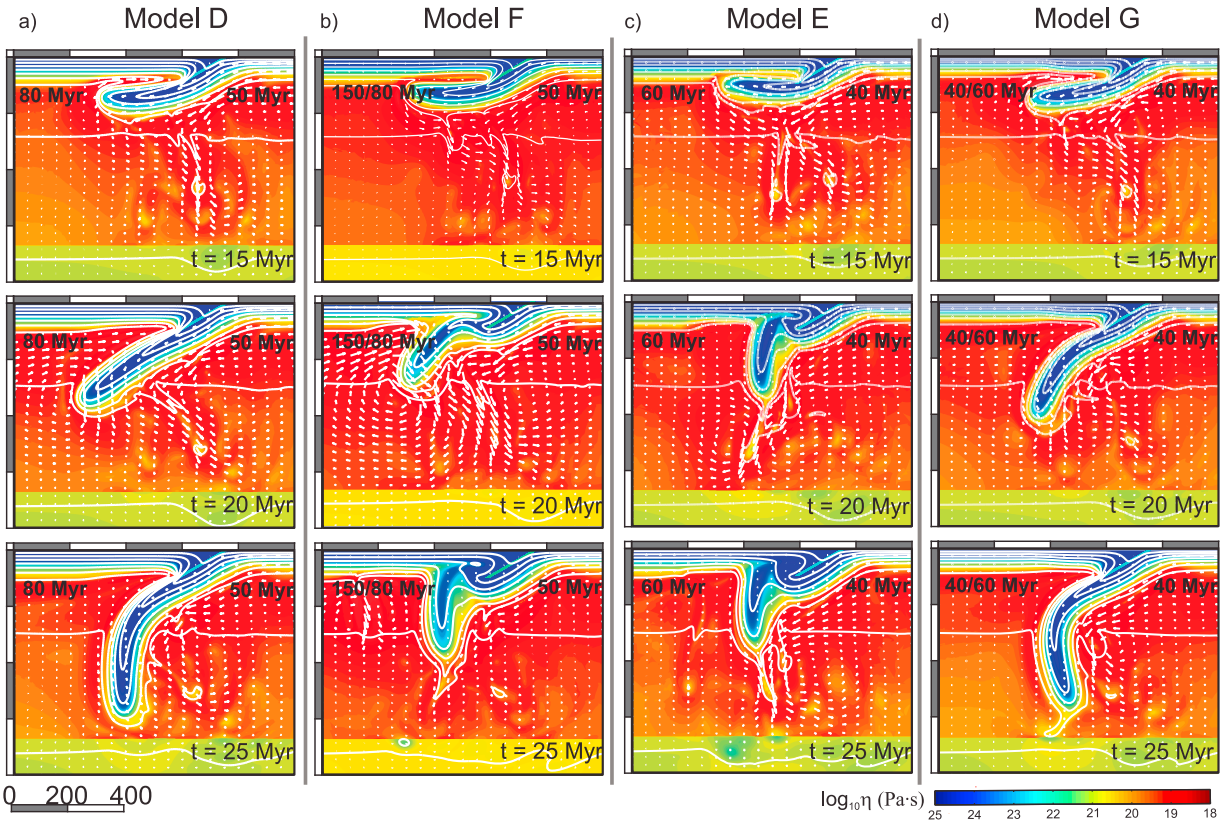

Figure 8. Model results at three different evolution times for simulations with (a) subducting plate of 50 Myr and an overriding plate of 80 Myr, Model D; (b) a subducting plate of 50 Myr and an overriding plate that changes age from 80 Myr (0–200 km from trench) to 150 Myr (>200 km from trench), Model F); (c) a subducting plate age of 40 Myr and an overriding plate with uniform age of 60 Myr, Model E; and (d) a subducting plate age of 40 Myr and an overriding plate that changes age from 60 Myr (0–200 km from trench) to 40 Myr (>200 km from trench), Model G. Decimal logarithm of the viscosity (color), isotherm every 200 degrees (contour) and velocity field (arrows) are shown.

40 Myr and A_{ov} = 60 Myr). Whereas Model E is an example of coupled subduction (see section 3.4.2, Figure 8c, and Animation S5), in Model G, when the slab reaches the portion of the overriding plate where the viscosity is lower, the suction torque starts decreasing, causing the gravitational torque to become dominant and the slab to become steeper (Figure 8d and Animation S7). In this situation the slab evolves to a profile with a long, low angle segment, followed by a steep segment. This simulation provides a possible explanation for the steep deepest portion of the slab in southern Mexico (profile A in Figure 9), which we consider further below.

[45] The sudden changes of overriding plate age imposed in this section should be considered as a modeling artifact intended to account for the first order effects of the proximity of cratons (cold lithosphere) or rift basins (hot lithosphere).

3.4.4. Role of Plate Coupling and Slab Strength

[46] We have performed a systematic analysis of the role of both plate ages. However, the characteristics of the modeled plate boundary and the rheology are also expected to have a significant role on the subduction style. In this section, we do not intend to systematically analyze the role of plate coupling or slab strength on subduction dynamics, which has been done elsewhere [e.g., *Billen and Hirth*, 2005, 2007; *De Franco et al.*, 2007], but to check whether the predicted influence of the upper plate thermal state is a general result, not restricted to a particular choice of parameters. For this purpose we have conducted an additional set of models where the coupling between both plates at the shear zone is decreased by reducing the maximum viscosity of the shear zone ($\eta_b = 10^{21}$ Pa·s), and the maximum overall viscosity cut-off is reduced ($\eta_{max} = 10^{24}$ Pa·s). For these models there is still a strong influ-

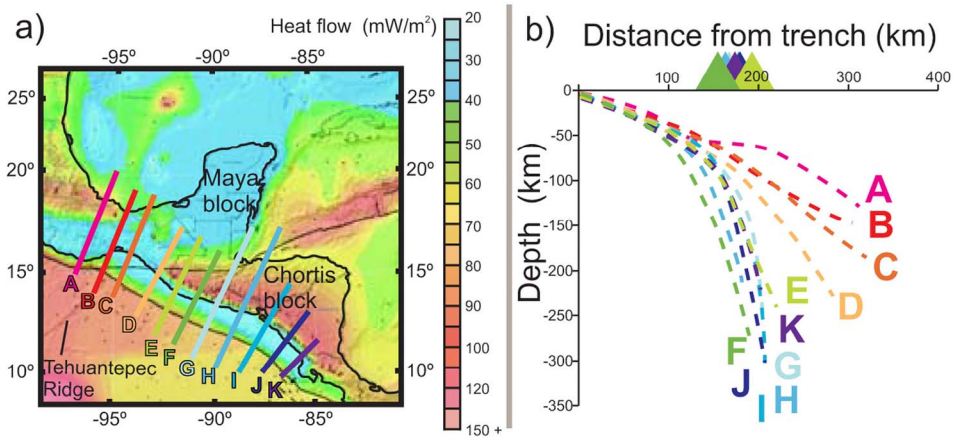

Figure 9. Heat flow and slab dip for the Cocos plate section of the Central American Trench. (a) Surface heat flow in Central America [*Blackwell and Richards*, 2004] and location of cross sections in Figure 9b. (b) Comparison between the slab dip profiles traced along the upper limits of the seismicity in the sections shown in Figure 9a [from *Álvarez-Gómez*, 2009] Triangles show the location of the volcanic arc for profiles E-K (volcanic arc is missing for profiles A-D).

ence of the thermal state of the overriding plate on the geometry of subduction (Models H–J, shown in Figure S1), especially for young subducting plates. In these weaker models (and with a weaker shear zone) the slab dip is steeper (for the same plate ages as in the models shown above). In contrast to the results presented for models with stronger slabs, in this case the variation of the slab dip with the overriding plate age is only gradual for the shallowest portion of the slab (between 100 and 200 km) and two distinct styles are reproduced. If the overriding plate is old (Model H), the hydrodynamic suction is so high that both plates become completely coupled and the plate cannot subduct. On the contrary, for younger overriding plates (Model I) the mean dip angle computed between 300 and 400 km is almost vertical. In these simulations, flat slab segments are also reproduced (Model J), but have a shorter duration and are much shorter in length because the gravitational torque causes these weaker slabs to steepen more rapidly.

[47] Unlike a rigid slab [e.g., *Stevenson and Turner*, 1977] flattening of the slab occurs because it is weak enough to deform in response to the changes in hydrodynamic stresses, while at the same time strong enough to support a substantial portion of its own weight. If the slab is too weak, it will either sink vertically or couple to the upper plate (if the hydrodymanic torque is strong enough), whereas if it is too strong the hydrodynamic stresses will not be able to deform it.

[48] Another important factor influencing plate coupling is the angle imposed for the shear zone. We have run several models in which we reduced the shear zone angle (θ_{sz}) to values of 25°, 20° and 15°, and obtained the same qualitative results, although these lower values of θ_{sz} promote the occurrence of shallow dip and flat subduction due to the increased plate coupling.

[49] We have tested the effect of subduction velocity. Equation (5) predicts a higher hydrodynamic suction for higher subduction velocities. However, the effect of the viscosity reduction due to the increased strain rate becomes predominant for sufficiently high subduction velocity values. For a velocity of 7.5 cm/yr (Models K and L, not shown), the induced flow is stronger and the viscosity is reduced, leading to steeper slabs (Model D versus K) and preventing coupling (Model E versus L). If on the contrary a slower subduction velocity (2.5 cm/yr) is used (Models M and N) the corner flow induced on the mantle wedge is decreased and therefore, the strain rate on that region is reduced. This leads to an increased viscosity that increases the coupling between the plates, resulting in decreased slab dips (Model B versus M) or even coupled subduction (Model C versus N).

[50] These tests show that, as expected, subduction style is also sensitive to the slab strength and to the amount of coupling at the plate boundary. We infer that flat subduction style is favored by moderate plate coupling and by a relatively stiff slab, however constraining the exact value of these parameters requires further study using fully dynamic 3D models. The 2D approach used here necessarily requires a kinematic boundary condition to reproduce flat and low angle subduction styles. On the other hand, present 3D models of free subduction introduce an initial perturbation (subducting plate

bending into the mantle) in order to develop self-sustained subduction and therefore evolve to high angle subduction [e.g., *Funiciello et al.*, 2003; *Stegman et al.*, 2006; *Di Giuseppe et al.*, 2008; *Yamato et al.*, 2009]. Future 3D models of self-sustained subduction should include variations of thermal state of the overriding plate along the trench to test its influence on slab dip.

4. Comparison to Cocos Plate Subduction

[51] To illustrate the influence of the thermal state of the overriding plate on slab dip, we discuss the variations of slab dip under southwestern Mexico and northern Central America and compare these to the modeling predictions (Figure 9). The subduction angle of the young (15–30 Myr old) Cocos plate under the Caribbean Plate deviates from the expected trend and is anomalously high for its age (Figure 1a, COST and Figure 1b, Central America). Moreover, the variability of the slab dip is very large, from 60 to 90 degrees in the deepest region, along this subduction zone, even for similar ages of the subducting plate (Figure 9b [from *Álvarez-Gómez*, 2009]). The slab profiles, from northwest to southeast, show flat subduction under southwestern Mexico (cross section A [see also, e.g., *Pardo and Suárez*, 1995]) low angle subduction (cross sections B-D) and high angle subduction (cross sections E-K). It is worthwhile noting the absence of a volcanic arc in cross-sections A-D. Several explanations can be given to explain this variability:

[52] 1. High slab dips have been explained as a result of the retreating motion of the overriding plate. This explanation is not suitable for the subduction under the Caribbean plate as this plate moves trenchward [*Gripp and Gordon*, 2002], which favors flat subduction [e.g., *van Hunen et al.*, 2004].

[53] 2. Another factor favoring steep dip is the increased toroidal flow around the edges of the slab. However, in Figures 1c and 1d, data from near-edge slabs from the studies by *Lallemand et al.* [2005] and *Cruciani et al.* [2005] have already been removed and this 'anomalous' steep dip is still found in both studies. Moreover cross sections E-I are far from edges and show high dip (Figure 9a).

[54] 3. Flat subduction has been explained in terms of the presence of anomalously buoyant material on the subducting plate [e.g., *Gutscher et al.*, 2000; *van Hunen et al.*, 2004], but the only buoyant material in this area is the Tehuantepec Ridge; and a single, small, ridge is not sufficient to produce flat subduction [*van Hunen et al.*, 2004].

[55] 4. Slab dip variability has also been suggested to be correlated with the stress-state or nature (continental versus oceanic) of the overriding plate [*Lallemand et al.*, 2005] or to the viscosity structure of the mantle wedge [e.g., *Manea and Gurnis*, 2007]. Here we provide an alternative, plausible explanation for the slab dip variability of the Cocos plate in terms of the variation of the thermal structure of the overriding plates and its relation with the hydrodynamic suction torque.

[56] The Maya (Yucatan) block of the North America plate is known to be of continental origin and was rotated to reach its current location after the opening of the Gulf of Mexico during the Late Jurassic [*Marton and Buffler*, 1994]. The Chortis block (Honduras, Nicaragua and Guatemala) of the Caribbean plate has been traditionally regarded as a Precambrian–Paleozoic continental nucleus previously attached to Southwestern Mexico. This terrain was translated from west to east and rotated counterclockwise during the Cenozoic [*Pindell and Barrett*, 1990]. While the Maya block is homogeneous [*Dickinson and Lawton*, 2001], the Chortis block is divided into different tectonic terrains including normal continental terrains, attenuated continental crust and oceanic terrains [*Rogers*, 2003]. Therefore, while the Maya block is part of a thick continental plate, the Chortis block is either formed of oceanic or thinned continental lithosphere. This structural variation is reflected in the surface heat flow map of the area, which exhibits much higher heat flow under the Chortis block compared to the Maya block (Figure 9a) and in lithospheric thickness maps [e.g., *Artemieva*, 2006], which show thickness of 50–100 km beneath the Chortis block compared to 100–125 km beneath the Maya block. Moreover, this transition corresponds with the North America-Caribbean plate boundary.

[57] The abrupt change in the surface heat flow between Maya block and the Chortis block reveals the contrast in thermal state between both plates, which involves a strong variation of the viscosity at the base of both plates close to the plate boundary interface at the mantle wedge (i.e., excluding the cold fore-arc mantle). This variation in thermal state corresponds to a transition from shallow slab dip in sections A-C to more steeply dipping profiles in sections D-K. On the basis of our modeling, we suggest that flat subduction of the Cocos plate under the colder Maya block is likely related to the

higher viscosity close to the base of the overriding plate (similar to Model D in Figures 3d and 4d), while subduction under the warmer Chortis block is much steeper due to reduced suction torque associated with a lower viscosity at the base of the upper plate (similar to Model A in Figures 3a and 4a).

[58] One may argue that this is a circular argument, as the observed variation in heat flow could simply reflect the current geometry of the slabs, with shallow-dipping slabs insulating the base of the lithosphere and steeply dipping slabs allowing for active mantle-wedge flow and volcanism leading to higher surface heat flow. First, the wavelength of the high surface heat flow in the Chortis block is too long to be related only to volcanism. More importantly, the differing tectonic history and terrane types of the Maya and Chortis blocks, and lithosphere thickness observations indicate that the present-day heat flow reflects the pre-existing structure of the subduction zone, which may have been reinforced by the subsequent differing evolution of the slab segments under each region.

[59] Finally, it is important to note that while subduction has been long-lived along the Central America Trench, there is evidence for recent detachment of the deeper portion of the slab [*Rogers et al.*, 2002], which would make the shallow portion of the slab more sensitive to variations of hydrodynamic forces. This observation is therefore also consistent with the model results, which show that episodes of flat slab subduction occur early in subduction when the slab has not yet entered the lower mantle.

5. Conclusions

[60] In order to test the influence of the thermal state of the overriding and subducting plates on the dynamics and geometry of subduction, we have developed a systematic study in which we vary separately the age of both plates. Our results indicate that, as expected from consideration of the gravitational torque, old subducting plates start subducting with a higher angle than young plates, due to higher negative buoyancy. However, the influence of the thermal state of the subducting lithosphere is only significant for the first stages of subduction, while the slab sinks into the upper mantle, and diminishes with time as slab geometry tends to reach steady state.

[61] In contrast, the influence of thermal state of the overriding plate on slab dip can have a noticeable effect on slab dip even for long evolution times, as colder overriding plates impart a higher viscosity at the base of the plate, and thus a higher hydrodynamic suction torque. Therefore, plates subducting underneath cold overriding plates are predicted to subduct with lower slab dip, and this effect is predicted to be more important than that of the subducting lithosphere age.

[62] Finally, with this simple modeling, varying only the age of the subducting and overriding plates we have been able to reproduce a wide range of slab geometries and different styles of subduction, including flat, low-angle and high-angle subduction.

[63] We compare our modeling predictions, in qualitative terms, with the Cocos slab dip variability beneath Central America. We provide a plausible explanation for this variability in terms of the change of the thermal state of the overriding plates, with flat subduction occurring under the cold lithosphere of the Maya block of North America and steep subduction under the warmer lithosphere of the Chortis block of the Caribbean plate.

Acknowledgments

[64] We would like to thank Susanne Buiter and an anonymous reviewer for thorough and constructive reviews, which helped to improve the manuscript. This work was funded by the Spanish Plan Nacional del MCINN project CGL2009–13103. This is a contribution of the Consolider-Ingenio 2010 team CSD2006–00041 (TOPO-IBERIA). J. Rodríguez-González acknowledges the support from Spanish Ministry of Education for a Ph.D grant and additional funding for a 4-month stage at UC-Davis. M. I. Billen acknowledges support from NSF grants 6877321 and 0748818.

References

Álvarez-Gómez, J. A. (2009), Tectónica Activa y Geodinámica en el Norte de Centroamérica, Ph.D. thesis, Univ. Complutense de Madrid, Madrid.

Arcay, D., S. Lallemand, and M.-P. Doin (2008), Back-arc strain in subduction zones: Statistical observations versus numerical modeling, *Geochem. Geophys. Geosyst.*, *9*, Q05015, doi:10.1029/2007GC001875.

Artemieva, I. M. (2006), Global 1° × 1° thermal model TC1 for the continental lithosphere: Implications for lithosphere secular evolution, *Tectonophysics*, *416*, 245–277, doi:10.1016/j.tecto.2005.11.022.

Barazangi, M., and B. L. Isacks (1979), Subduction of the Nazca plate beneath Peru: Evidence from spatial distribution of earthquakes, *Geophys. J. R. Astron. Soc.*, *57*(3), 537–555.

Bellahsen, N., C. Faccenna, and F. Funiciello (2005), Dynamics of subduction and plate motion in laboratory experiments: Insights into the "plate tectonics" behavior of the Earth, *J. Geophys. Res.*, *110*, B01401, doi:10.1029/2004JB002999.

Billen, M. I. (2008), Modeling the dynamics of subducting Slabs, *Annu. Rev. Earth Planet. Sci.*, *36*, 325–356, doi:10.1146/annurev.earth.36.031207.124129.

Billen, M. I., and G. Hirth (2005), Newtonian versus non-Newtonian upper mantle viscosity: Implications for subduction initiation, *Geophys. Res. Lett.*, *32*, L19304, doi:10.1029/2005GL023457.

Billen, M. I., and G. Hirth (2007), Rheologic controls on slab dynamics, *Geochem. Geophys. Geosyst.*, *8*, Q08012, doi:10.1029/2007GC001597.

Bird, P. (1988), Formation of the Rocky Mountains, western United States: A continuum computer model, *Science*, *239*(4847), 1501–1507, doi:10.1126/science.239.4847.1501.

Blackwell, D., and M. Richards (2004), *Geothermal Map of North America*, Am. Assoc. Petrol. Geol., Tulsa, Okla.

Boutelier, D. A., and A. R. Cruden (2008), Impact of regional mantle flow on subducting plate geometry and interplate stress: Insights from physical modelling, *Geophys. J. Int.*, *174*, 719–732, doi:10.1111/j.1365-246X.2008.03826.x.

Buffett, B. A., and D. B. Rowley (2006), Plate bending at subduction zones: Consequences for the direction of plate motions, *Earth Planet. Sci. Lett.*, *245*(1–2), 359–364, doi:10.1016/j.epsl.2006.03.011.

Burkett, E., and M. I. Billen (2009), Dynamics and implications of slab detachment due to ridge-trench collision, *J. Geophys. Res.*, *114*, B12402, doi:10.1029/2009JB006402.

Capitanio, F. A., D. R. Stegman, L. N. Moresi, and W. Sharples (2010), Upper plate controls on deep subduction, trench migrations and deformations at convergent margins, *Tectonophysics*, *483*(1–2), 80–92, doi:10.1016/j.tecto.2009.08.020.

Carslaw, H. S., and J. C. Jaeger (1984), *Conduction of Heat in Solids*, Clarendon, Oxford, U. K.

Chen, J., and S. D. King (1998), The influence of temperature and depth dependent viscosity on geoid and topography profiles from models of mantle convection, *Phys. Earth Planet. Inter.*, *106*, 75–92, doi:10.1016/S0031-9201(97)00110-6.

Christensen, U. R. (1996), The influence of trench migration on slab penetration into the lower mantle, *Earth Planet. Sci. Lett.*, *140*, 27–39, doi:10.1016/0012-821X(96)00023-4.

Christeson, G. L., S. P. S. Gulick, H. J. A. van Avendonk, L. L. Worthington, R. S. Reece, and T. L. Pavlis (2010), The Yakutat Terrane: Dramatic change in crustal thickness across the Transition Fault, Alaska, *Geology*, *38*(10), 895–898, doi:10.1130/G31170.1.

Čížková, H., J. van Hunen, A. P. van den Berg, and N. J. Vlaar (2002), The influence of rheological weakening and yield stress on the interaction of slabs with the 670 km discontinuity, *Earth Planet. Sci. Lett.*, *199*(3–4), 447–457, doi:10.1016/S0012-821X(02)00586-1.

Conrad, C. P., and B. H. Hager (1999), Effects of plate bending and fault strength at subduction zones on plate dynamics, *J. Geophys. Res.*, *104*(B8), 17,551–17,571, doi:10.1029/1999JB900149.

Conrad, C. P., and C. Lithgow-Bertelloni (2002), How mantle slabs drive plate tectonics, *Science*, *298*, 207–209, doi:10.1126/science.1074161.

Conrad, C. P., and C. Lithgow-Bertelloni (2004), The temporal evolution of plate driving forces: Importance of "slab suction" versus "slab pull" during the Cenozoic, *J. Geophys. Res.*, *109*, B10407, doi:10.1029/2004JB002991.

Cruciani, C., E. Carminati, and C. Doglioni (2005), Slab dip vs. lithosphere age: No direct function, *Earth Planet. Sci. Lett.*, *238*, 298–310, doi:10.1016/j.epsl.2005.07.025.

De Franco, R., R. Govers, and R. Wortel (2007), Numerical comparison of different convergent plate contacts: Subduction channel and subduction fault, *Geophys. J. Int.*, *171*, 435–450, doi:10.1111/j.1365-246X.2006.03498.x.

Di Giuseppe, E., J. van Hunen, F. Funiciello, C. Faccenna, and D. Giardini (2008), Slab stiffness control of trench motion: Insights from numerical models, *Geochem. Geophys. Geosyst.*, *9*, Q02014, doi:10.1029/2007GC001776.

Dickinson, W., and T. Lawton (2001), Carboniferous to Cretaceous assembly and fragmentation of Mexico, *Geol. Soc. Am. Bull.*, *113*, 1142–1160.

Doglioni, C., P. Harabaglia, S. Merlini, F. Mongelli, A. Peccerillo, and C. Piromallo (1999), Orogens and slabs vs. their direction of subduction, *Earth Sci. Rev.*, *45*, 167–208, doi:10.1016/S0012-8252(98)00045-2.

Eberle, M. A., A. Grasset, and C. Sotin (2002), A numerical study of the interaction between the mantle wedge, subducting slab, and overriding plate, *Phys. Earth Planet. Inter.*, *134*, 191–202, doi:10.1016/S0031-9201(02)00157-7.

Enns, A., T. W. Becker, and H. Schmeling (2005), The dynamics of subduction and trench migration for viscosity stratification, *Geophys. J. Int.*, *160*, 761–775, doi:10.1111/j.1365-246X.2005.02519.x.

Faccenda, M., T. V. Gerya, and L. Burlini (2009), Deep slab hydration induced by bending-related variations in tectonic pressure, *Nat. Geosci.*, *2*, 790–793, doi:10.1038/ngeo656.

Faccenna, C., A. Heuret, F. Funiciello, S. Lallemand, and T. W. Becker (2007), Predicting trench and plate motion from the dynamics of a strong slab, *Earth Planet. Sci. Lett.*, *257*, 29–36, doi:10.1016/j.epsl.2007.02.016.

Funiciello, F., C. Faccenna, D. Gardini, and K. Regenauer-Lieb (2003), Dynamics of retreating slabs: 2. Insights from three-dimensional laboratory experiments, *J. Geophys. Res.*, *108*(B4), 2207, doi:10.1029/2001JB000896.

Funiciello, F., M. Moroni, C. Piromallo, C. Faccenna, A. Cenedese, and H. Bui (2006), Mapping mantle flow during retreating subduction: Laboratory models analyzed by feature tracking, *J. Geophys. Res.*, *111*, B03402, doi:10.1029/2005JB003792.

Funiciello, F., C. Faccenna, A. Heuret, S. Lallemand, E. D. Giuseppe, and T. W. Becker (2008), Trench migration, net rotation and slab–mantle coupling, *Earth Planet. Sci. Lett.*, *271*, 233–240, doi:10.1016/j.epsl.2008.04.006.

Griffiths, R. W., R. I. Hackney, and R. D. van der Hilst (1995), A laboratory investigation of effects of trench migration on the descent of subducted slabs, *Earth Planet. Sci. Lett.*, *133*, 1–17, doi:10.1016/0012-821X(95)00027-A.

Gripp, A. E., and R. G. Gordon (2002), Young tracks of hotspots and current plate velocities, *Geophys. J. Int.*, *150*, 321–361, doi:10.1046/j.1365-246X.2002.01627.x.

Guillou-Frottier, L., J. Buttles, and P. Olson (1995), Laboratory experiments on structure of subducted lithosphere, *Earth Planet. Sci. Lett.*, *19*(5), 814–833.

Gutscher, M.-A., W. Spakman, H. Bijwaard, and E. R. Engdahl (2000), Geodynamics of flat subduction: Seismicity and tomographic constraints from the Andean margin, *Tectonics*, *19*(5), 814–833, doi:10.1029/1999TC001152.

Han, L., and M. Gurnis (1999), How valid are dynamic models of subduction and convection when plate motions are prescribed?, *Phys. Earth Planet. Inter.*, *110*, 235–246, doi:10.1016/S0031-9201(98)00156-3.

Heuret, A., F. Funiciello, C. Faccenna, and S. Lallemand (2007), Plate kinematics, slab shape and back-arc stress: A comparison between laboratory models and current subduction zones, *Earth Planet. Sci. Lett.*, *256*, 473–483, doi:10.1016/j.epsl.2007.02.004.

Hirth, G., and D. Kohlstedt (2003), Rheology of the upper mantle and the mantle wedge: A view from the experimentalists, in *Inside the Subduction Factory*, edited by J. Eiler, pp. 83–105, AGU, Washington, D. C., doi:10.1029/138GM06.

Isacks, B. L., and M. Barazangi (1977), Geometry of Benioff zones: Lateral segmentation and downwards bending of the subducted lithosphere, paper presented at Symposium on Island Arcs, Deep Sea Trenches and Back-Arc Basins, AGU, New York.

Ita, J., and S. D. King (1994), Sensitivity of convection with an endothermic phase change to the form of governing equations, initial conditions, boundary conditions and equation of state, *J. Geophys. Res.*, *99*, 15,919–15,938, doi:10.1029/94JB00852.

Jarrard, R. D. (1986), Relations among subduction parameters, *Rev. Geophys.*, *24*(2), 217–284, doi:10.1029/RG024i002p00217.

Jischke, M. C. (1975), On the dynamics of descending lithospheric plates and slip zones, *J. Geophys. Res.*, *80*, 4809–4813, doi:10.1029/JB080i035p04809.

Kincaid, C., and P. Olson (1987), An experimental study of subduction and slab migration, *J. Geophys. Res.*, *92*(B13), 13,832–13,840, doi:10.1029/JB092iB13p13832.

Kincaid, C., and I. S. Sacks (1997), Thermal and dynamical evolution of the upper mantle in subduction zones, *J. Geophys. Res.*, *102*, 12,295–12,315, doi:10.1029/96JB03553.

King, S. D. (2001), Subduction zones: Observations and geodynamic models, *Phys. Earth Planet. Inter.*, *127*, 9–24, doi:10.1016/S0031-9201(01)00218-7.

King, S. D. (2007), Downwellings and the fate of subducting slabs: Constraints from seismology, geoid, topography, geochemistry, and petrology, in *Treatise in Geophysics*, vol. 3, *Mantle Dynamics*, edited by D. Bercovici, chap. 8, pp. 325–370, Elsevier, Boston, Mass., doi:10.1016/B978-044452748-6/00122-X.

Kukačka, M., and C. Matyska (2004), Influence of the zone of weakness on dip angle and shear heating of subducted slabs, *Earth Phys. Planet. Inter.*, *141*, 243–252, doi:10.1016/j.pepi.2003.11.004.

Lallemand, S., A. Heuret, and D. Boutelier (2005), On the relationships between slab dip, back-arc stress, upper plate absolute motion, and crustal nature in subduction zones, *Geochem. Geophys. Geosyst.*, *6*, Q09006, doi:10.1029/2005GC000917.

Manea, V., and M. Gurnis (2007), Subduction zone evolution and low viscosity wedges and channels, *Earth Planet. Sci. Lett.*, *264*, 22–45, doi:10.1016/j.epsl.2007.08.030.

Marton, G., and R. Buffler (1994), Jurrassic reconstruction of the Gulf of Mexico basin, *Int. Geol. Rev.*, *36*, 545–586, doi:10.1080/00206819409465475.

McKenzie, D. P. (1967), Some remarks on heat flow and gravity anomalies, *J. Geophys. Res.*, *72*, 6261–6273, doi:10.1029/JZ072i024p06261.

McKenzie, D. P. (1969), Speculations on the consequences and causes of plate motions, *Geophys. J. R. Astron. Soc.*, *18*, 1–32.

O'Driscoll, L. J., E. D. Humphreys, and F. Saucier (2009), Subduction adjacent to deep continental roots: Enhanced negative pressure in the mantle wedge, mountain building and continental motion, *Earth Planet. Sci. Lett.*, *280*(1–4), 61–70, doi:10.1016/j.epsl.2009.01.020.

Olbertz, D., and M. J. R. Wortel (1997), Trench migration and subduction zone geometry, *Geophys. Res. Lett.*, *24*(3), 221–224, doi:10.1029/96GL03971.

Oxburgh, E., and D. L. Turcotte (1978), Mechanisms of continental drift, *Rep. Prog. Phys.*, *41*, 1249–1312.

Pardo, M., and G. Suárez (1995), Shape of the subducted Rivera and Cocos plates in Southern Mexico: Seismic and tectonic implications, *J. Geophys. Res.*, *100*(B7), 12,357–12,373, doi:10.1029/95JB00919.

Pérez-Campos, X., Y. Kim, A. Husker, P. M. Davis, R. W. Clayton, A. Iglesias, J. F. Pacheco, S. K. Singh, V. C. Manea, and M. Gurnis (2008), Horizontal subduction and truncation of the Cocos plate beneath central Mexico, *Geophys. Res. Lett.*, *35*, L18303, doi:10.1029/2008GL035127.

Pérez-Gussinyé, M., A. R. Lowry, J. Phipps Morgan, and A. Tassara (2008), Effective elastic thickness variations along the Andean margin and their relationship to subduction geometry, *Geochem. Geophys. Geosyst.*, *9*, Q02003, doi:10.1029/2007GC001786.

Pindell, J. L., and S. F. Barrett (1990), Geologic evolution of the Caribbean: A plate-tectonic perspective, in *The Geology of North America*, vol. H, *The Caribbean Region*, edited by G. Dengo and J. E. Case, pp. 405–432, Geol. Soc. of Am., Boulder, Colo.

Piromallo, C., T. W. Becker, F. Funiciello, and C. Faccenna (2006), Three-dimensional instantaneous mantle flow induced by subduction, *Geophys. Res. Lett.*, *33*, L08304, doi:10.1029/2005GL025390.

Quinquis, M. E. T., S. J. H. Buiter, and S. Ellis (2011), The role of boundary conditions in numerical models of subduction zone dynamics, *Tectonophysics*, *497*, 57–70, doi:10.1016/j.tecto.2010.11.001.

Ribe, N. M. (2010), Bending mechanics and mode selection in free subduction: A thin-sheet analysis, *Geophys. J. Int.*, *180*(2), 559–576, doi:10.1111/j.1365-246X.2009.04460.x.

Ricard, Y., C. Doglioni, and R. Sabadini (1991), Differential rotation between lithosphere and mantle: A consequence of lateral mantle variations, *J. Geophys. Res.*, *96*, 8407–8415, doi:10.1029/91JB00204.

Riguzzi, F., G. Panza, P. Varga, and C. Doglioni (2009), Can Earth's rotation and tidal despinning drive plate tectonics?, *Tectonophysics*, *484*, 60–73.

Roda, M., A. M. Marotta, and M. I. Spalla (2011), The effects of the overriding plate thermal state on the slab dip in an ocean-continent subduction system, *C. R. Geosci.*, *343*, 323–330, doi:10.1016/j.crte.2011.01.005.

Rogers, R. (2003), *Jurassic–Recent Tectonic and Stratigraphic History of the Chortis Block of Honduras and Nicaragua*, Univ. of Tex., Austin.

Rogers, R. D., H. Karason, and R. D. van der Hilst (2002), Epeirogenic uplift above a detached slab in northern Central America, *Geology*, *30*(11), 1031–1034, doi:10.1130/0091-7613(2002)030<1031:EUAADS>2.0.CO;2.

Royden, L. H., and L. Husson (2006), Trench motion, slab geometry and viscous stresses in subduction systems, *Geophys. J. Int.*, *167*, 881–905, doi:10.1111/j.1365-246X.2006.03079.x.

Schellart, W. P. (2004), Kinematics of subduction and subduction-induced flow in the upper mantle, *J. Geophys. Res.*, *109*, B07401, doi:10.1029/2004JB002970.

Schellart, W. P. (2007), The potential influence of subduction zone polarity on overriding plate deformation, trenchmigration and slab dip angle, *Tectonophysics*, *445*, 363–372, doi:10.1016/j.tecto.2007.09.009.

Schellart, W. P., J. Freeman, D. R. Stegman, L. Moresi, and D. May (2007), Evolution and diversity of subduction zones controlled by slab width, *Nature*, *446*, 308–311, doi:10.1038/nature05615.

Schenk, O., and K. Gärtner (2004), Solving unsymmetric sparse systems of linear equations with PARDISO, *Future*

Gener. Comput. Syst., *20*(3), 475–487, doi:10.1016/j.future.2003.07.011.

Schenk, O., and K. Gärtner (2006), On fast factorization pivoting methods for symmetric indefinite systems, *Electron. Trans. Numer. Anal.*, *23*, 158–179.

Schmeling, H., R. Monz, and D. C. Rubie (1999), The influence of olivine metastability on the dynamics of subduction, *Earth Planet. Sci. Lett.*, *165*, 55–66, doi:10.1016/S0012-821X(98)00249-0.

Schmid, C., S. Goes, S. van der Lee, and D. Giardini (2002), Fate of the Cenozoic Farallon slab from a comparison of kinematic thermal modeling with tomographic images, *Earth Planet. Sci. Lett.*, *204*, 17–32, doi:10.1016/S0012-821X(02)00985-8.

Schubert, G., D. L. Turcotte, and P. Olson (2001), *Mantle Convection in the Earth and Planets*, Cambridge Univ. Press, Cambridge, U. K., doi:10.1017/CBO9780511612879.

Sigloch, K., N. McQuarrie, and G. Nolet (2008), Two-stage subduction history under North America inferred from multiple-frequency tomography, *Nat. Geosci.*, *1*, 458–462, doi:10.1038/ngeo231.

Stegman, D. R., J. Freeman, W. P. Schellart, L. Moresi, and D. May (2006), Influence of trench width on subduction hinge retreat rates in 3-D models of slab rollback, *Geochem. Geophys. Geosyst.*, *7*, Q03012, doi:10.1029/2005GC001056.

Stegman, D. R., R. Farrington, F. A. Capitanio, and W. P. Schellart (2010), A regime diagram for subduction styles from 3-D numerical models of free subduction, *Tectonophysics*, *483*, 29–45, doi:10.1016/j.tecto.2009.08.041.

Stein, C. A., and S. A. Stein (1992), A model for the global variation in oceanic depth and heat flow with lithospheric age, *Nature*, *359*, 123–129, doi:10.1038/359123a0.

Stevenson, D. J., and J. S. Turner (1977), Angle of subduction, *Nature*, *270*(5635), 334–336, doi:10.1038/270334a0.

Suárez, G., T. Monfret, and G. Wittlinger (1990), Geometry of subduction and depth of the seismogenic zone in the Guerero gap, Mexico, *Nature*, *345*, 336–338, doi:10.1038/345336a0.

Tetzlaff, M., and H. Schmeling (2000), The influence of olivine metastability on deep subduction of oceanic lithosphere, *Phys. Earth Planet. Inter.*, *120*(1–2), 29–38, doi:10.1016/S0031-9201(00)00139-4.

Tetzlaff, M., and H. Schmeling (2009), Time-dependent interaction between subduction dynamics and phase transition kinetics, *Geophys. J. Int.*, *178*(2), 826–844, doi:10.1111/j.1365-246X.2009.04182.x.

Tovish, A., G. Schubert, and B. P. Luyenduk (1978), Mantle flow pressure and the angle of subduction: Non-Newtonian corner flows, *J. Geophys. Res.*, *83*(B12), 5892–5898, doi:10.1029/JB083iB12p05892.

Uyeda, S., and H. Kanamori (1979), Back arc opening and the mode of subduction, *J. Geophys. Res.*, *84*, 1049–1061, doi:10.1029/JB084iB03p01049.

van Dinther, Y., G. Morra, F. Funiciello, and C. Faccenna (2010), Role of the overriding plate in the subduction process: Insights from numerical models, *Tectonophysics*, *484*, 74–86, doi:10.1016/j.tecto.2009.08.038.

van Hunen, J., A. P. van den Berg, and N. J. Vlaar (2001), Latent heat effects of the major mantle phase transitions on low-angle subduction, *Earth Planet. Sci. Lett.*, *190*(3–4), 125–135, doi:10.1016/S0012-821X(01)00383-1.

van Hunen, J., A. P. van den Berg, and N. J. Vlaar (2002a), The impact of the South-American plate motion and the Nazca Ridge subduction on the flat subduction below South Peru, *Geophys. Res. Lett.*, *29*(14), 1690, doi:10.1029/2001GL014004.

van Hunen, J., A. P. van den Berg, and N. J. Vlaar (2002b), On the role of subducting oceanic plateaus in the development of shallow flat subduction, *Tectonophysics*, *352*, 317–333, doi:10.1016/S0040-1951(02)00263-9.

van Hunen, J., A. P. van den Berg, and N. J. Vlaar (2004), Various mechanisms to induce present-day shallow flat subduction and implications for the younger Earth: A numerical parameter study, *Earth Planet. Sci. Lett.*, *146*, 179–194.

Yamato, P., L. Husson, J. Braun, C. Loiselet, and C. Thieulot (2009), Influence of surrounding plates on 3D subduction dynamics, *Geophys. Res. Lett.*, *36*, L07303, doi:10.1029/2008GL036942.

Zhong, S., and M. Gurnis (1995), Mantle convection with plates and mobile, faulted plate margins, *Science*, *267*, 838–843, doi:10.1126/science.267.5199.838.